Exp.-Nr.: A1/ –94
Eingang:
an PAC:

Mainz Microtron MAMI

Collaboration A1: "Virtual Photons"

Spokesperson: R. Neuhausen

Proposal for an Experiment

Threshold π^0 Electroproduction

Collaborators:

A.M. Bernstein*, H. Merkel, D. Newton
(Bates Linear Accelerator Center, Laboratory for Nuclear Science and Department of Physics, MIT, Cambridge)

W.U. Boeglin, R. Böhm, M.O. Distler, R. Edelhoff, J. Friedrich, R. Geiges, M. Kahrau, M. Korn, H. Kramer, K.W. Krygier, V. Kunde, A. Liesenfeld, R. Neuhausen, E.A.J.M. Offermann, Th. Pospischil, A.W. Richter, G. Rosner, P. Sauer, S. Schardt, A. Wagner, Th. Walcher*, S. Wolf
(Institut für Kernphysik, Universität Mainz)

M. Kuss, A. Richter, G. Schrieder, T. Suda
(Institut für Kernphysik, Technische Hochschule Darmstadt)

R. Miskimen
(Department of Physics and Astronomy, University of Massachusetts, Amherst)

B. Norum
(Department of Physics, University of Virginia, Charlottesville)

T.P. Welch
(Department of Physics, Oregon State University, Corvallis)

*Contact Persons

Abstract

We propose to investigate the threshold p($\vec{e}$,e'p)π^0 reaction at $q^2 = -0.05$ (GeV/c)^2 as a test of the predictions of chiral dynamics, a low energy approximation to QCD. The structure functions $\sigma_{\rm L}$ and $\sigma_{\rm T}$ are determined by a Rosenbluth separation, $\sigma_{\rm TL}$ and $\sigma_{\rm TT}$ by the Φ dependence of the cross section and $\sigma_{\rm TL'}$ will be measured by an out of plane measurement with polarized electrons. In addition we want to measure the q^2 dependence of the E_{0+} and L_{0+} multipole at $-q^2 < 0.1$ (GeV/c)^2.

1 Introduction

The fundamental nature of the pion photo and electroproduction processes at threshold has long been recognized [Am79]. This is due in part to the fact that the pion is the almost Goldstone boson of QCD [Do92]. Starting with the low energy theorems of current algebra [Ad68, We66] predictions for the s wave amplitudes for the $N(\gamma,\pi)$ [deB70, Na91] and $N(e,e'\pi)$ [Sc93] reactions have been made. Table 1 shows the results for the s wave longitudinal and transverse multipoles L_{0+} and E_{0+} [Sc93]. From this table one can see that the leading terms for the charged pion amplitudes are pion and nucleon form factors (the gauge invariant terms). We will take advantage of this to measure the axial form factor of the nucleon (F_A which contributes to the E_{0+} multipole) in the inclusive $p(e,e')n\pi^+$ reaction in some future experiment. By contrast the neutral pion amplitudes are proportional to the chiral symmetry breaking terms $\mu = m_\pi/M$ and are therefore much more sensitive to the dynamics of the hadron constituents now calculable in the framework of chiral perturbation theory. This is the reason that the $p(e,e'p)\pi^\circ$ channel is the main thrust of this proposal.

The effective field theory technique called chiral perturbation theory has been employed as a low energy approximations to QCD [We79]. The lowest, or tree level, approximation generally reproduces the results of current algebra to order μ. Chiral dynamics (or chiral perturbation theory) has been employed to calculate threshold photo- [Be92] and electro- [Be93] pion production. Since both the low energy theorems and chiral perturbation theory calculations follow from general principles it is very instructive to make precision tests of their predictions. The experimental tools for accurate measurements have only recently become available. The main new advances are CW electron and photon beams of high quality and polarization, along with improvements in detectors.

An important start in this field has been made with studies of the threshold $p(\gamma,\pi^0)$ reaction at Saclay [Ma86] and Mainz [Bec90]. The results of these experiments for the electric dipole amplitude E_{0+} at threshold [Ber91] are in agreement with the predictions of the low energy theorems and of chiral perturbation theory. However there are important questions still remaining about the interpretation of these data away from threshold (discussed in Sec. 3) which can be resolved by more accurate unpolarized cross section data and even more importantly by the use of polarized photons. Further experimental improvements will allow us to obtain the slope of the E_{0+} and the p wave multipoles. These quantities, which are even more sensitive to the dynamics, have been predicted by chiral perturbation theory [Be93] and by more conventional model calculations [No90].

The first successful study of the threshold $p(e,e'p)\pi^0$ reaction was performed at NIKHEF [We92]. Cross section results were obtained for q^2 between -0.05 and -0.1 $(GeV/c)^2$. CM energies up to 2.5 MeV above threshold were observed and the dominant contribution was for s wave pions. The results are in agreement with the predictions of chiral perturbation theory [Be93]. The experiment was severely limited by the low duty cycle (1%) and only $\approx$ 200 counts in the π^0 channel were observed. It is very important to obtain more accurate data over an extended energy region in order to measure the p wave pion emission and the energy dependence of the s wave amplitudes. As in the photoproduction case these important predictions of chiral perturbation theory are even more sensitive to the dynamics.

channel	E_{0+}
π^+	$\sqrt{2}(F_A - G_M^n \frac{\nu_2}{2-\nu_2} - \frac{1}{2}\mu + [\mu\nu_2, \mu^2])$
π^-	$\sqrt{2}(-F_A - G_M^p \frac{\nu_2}{2-\nu_2} - \frac{1}{2}\mu + [\mu\nu_2, \mu^2])$
$p\pi^0$	$-\mu + \frac{1}{2}\mu^2(1+\kappa^p) - G_M^p \frac{\nu_2}{2-\nu_2} + [\mu\nu_2, \mu^3]$
$n\pi^0$	$-\frac{1}{2}\mu^2\kappa^n + G_M^n \frac{\nu_2}{2-\nu_2} + [\mu\nu_2, \mu^3]$
channel	L_{0+}
π^+	$\sqrt{2}(\frac{\mu^2(1+\mu)}{\mu^2(2+\mu)-\nu_2} F^\pi - G_E^n \frac{\nu_2}{2-\nu_2} - \frac{1}{2}\mu + [\mu\nu_2, \mu^2])$
π^-	$\sqrt{2}(-\frac{\mu^2(1+\mu)}{\mu^2(2+\mu)-\nu_2} F^\pi - G_E^p \frac{\nu_2}{2-\nu_2} - \frac{1}{2}\mu + [\mu\nu_2, \mu^2])$
$p\pi^0$	$-\mu + \frac{1}{2}\mu^2 - G_E^p \frac{\nu_2}{2-\nu_2} + [\mu\nu_2, \mu^3]$
$n\pi^0$	$G_E^n \frac{\nu_2}{2-\nu_2} + [\mu\nu_2, \mu^3]$

Table 1: Threshold production amplitudes E_{0+} and L_{0+} [Sc93] in units of $C = \frac{eg}{2M}\frac{1}{4\pi(1+\mu)}\frac{1}{2}\sqrt{\frac{(2+\mu)^2-\nu_2}{1+\mu}}$ with $G_M = F_1 + F_2$, $G_E = F_1 + \frac{\nu_2}{4}F_2$, $\kappa^p = F_2^p(0) = 1.79$, $\kappa^n = F_2^n(0) = -1.91$. All form factors are functions of k^2. $\nu_2 = \frac{q^2}{M_p^2}$, $\mu = \frac{m_\pi}{M_p}$.

It is important to study electroproduction in addition to photoproduction for several reasons:

- there are additional longitudinal multipoles which are independent probes of the dynamics. In particular the σ_{TL} and $\sigma_{TL'}$ structure functions measure the relative phases of the longitudinal and transverse amplitudes and are therefore particularly sensitive to the dynamics;
- since the CM energy W can be varied independently of q^2 one now has two momentum scales to vary independently. Since chiral perturbation theory is an asymptotic expansion increasing the magnitudes of either p^*_π or the momentum transfer q this provides a greater challenge to the predictions.

If it turns out that these calculation work at low momenta it will be very interesting to see where they begin to disagree with experiment. For this experiment we have chosen a relatively modest value of $p^*_\pi < 100 MeV/c$ and $-q^2 < 0.1\ (GeV/c)^2$ since these values are approximately the maximum values that can be predicted by a 1 loop chiral perturbation theory calculation [Be93].

The proposed measurement is a continuation of the test measurement of the $p(e, e'p)\pi^\circ$ reaction at $q^2 = -0.1\ (GeV/c)^2$ that we started in 1994 [Di94]. The results of this experiment are presented in Sec. 5.

2 Cross Sections

The electroproduction amplitudes are functions of W (the CM energy of the πN system) and q^2

$$q^2 = -4\ E\ E'\ \sin^2\frac{\theta_e}{2} \tag{1}$$

$$W^2 = q^2\ +\ 2\omega M_p\ +\ M_p^2 \tag{2}$$

where E is the electron beam energy, θ_e is the electron scattering angle, E' is the scattered electron energy, and $\omega = E - E'$.

The cross section for the $p(e, e'\pi)p$ reaction can be written as

$$\frac{d^3\sigma}{d\Omega_e dE' d\Omega^*_\pi} = \Gamma_t[\sigma_T(\theta) + \epsilon\sigma_L(\theta) + \epsilon\sigma_{TT}(\theta)\cos 2\phi \tag{3}$$

$$+\sqrt{2\epsilon(1+\epsilon)}\sigma_{TL}(\theta)\cos\phi + h\sqrt{2\epsilon(1-\epsilon)}\sigma_{TL'}(\theta)\sin\phi]$$

where ϵ is the photon polarization parameter, Γ_t is the virtual photon flux, $h = \pm 1$ is the electron helicity, and ϕ is the out of plane angle for the detected hadron. Due to the kinematic focusing we will measure the ϕ dependence of the cross section at threshold within the acceptance of the proton spectrometer. For higher pion momenta we use the out of plane ability of the Mainz spectrometer setup. The σ_{TT} and σ_{TL} interference structure functions are measured on the basis of their ϕ dependence. The $\sigma_{TL'}$ structure function is obtained from its electron helicity dependence.

The relationship between the cross sections and the multipoles is given in the appendix. The scalar and transverse s wave multipoles S_{0+} and E_{0+} are the only ones that are finite at threshold. In the low momentum region the p wave multipoles all go to zero as p^*_π, CM pion momentum. Sufficiently close to threshold the p wave multipoles must be small; $\sigma_L \approx -\frac{q^2}{q^{*2}}|S_{0+}|^2$ and $\sigma_T \approx |E_{0+}|^2$ are almost isotropic and the interference structure functions become negligible. In this region it is sufficient to measure the total cross section for virtual photons

$$\frac{d^2\sigma}{d\Omega_e dE'} = \Gamma_t(\sigma_T + \epsilon\sigma_L) \approx 4\pi\Gamma_t\frac{p^*_\pi}{k^*_\gamma}(A_0 + bp^{*2}_\pi) \tag{4}$$

where

$$A_0 = |E_{0+}|^2 - \epsilon\frac{q^2}{q^{*2}}|S_{0+}|^2 \tag{5}$$

and k^*_γ is the CM photon energy. Note that Eqn. 5 can be written in terms of the longitudinal s wave multipole L_{0+} by using the relationship

$$\omega^* S_{0+} = q^* L_{0+} \tag{6}$$

where ω^* (q^*) are the electron energy loss (momentum transfer) in the CM system.

We shall use the inclusive electron scattering data that we will collect during the coincidence experiment to measure E_{0+} and S_{0+} for the $p(e, e')n\pi^+$ reaction.

	E_{0+} $[10^{-3}/m_\pi]$	L_{0+} $[10^{-3}/m_\pi]$
Experiment [We92]	$-1.9\ \pm 0.2$	$3.2\ \pm 1.2$
Low Energy Theorems [deB70,Sc93]	$-2.3\ \pm 0.2$	2.83
Chiral Perturbation Theory		
1 loop [Be92,Be93]	-1.33 ± 0.09	2.05
1 loop with isospin breaking [Me94]	-1.97	3.16

Table 2: $\gamma p \to \pi^0 p$ s wave photo and electro-production amplitudes.

3 Previous Experiments

The first threshold $p(\vec{e}, e'p)\pi^0$ experiment that obtained cross sections significantly different then zero was performed at NIKHEF [We92]. Data was obtained for CM energies up to $\Delta W = 1.5\ MeV$ above threshold for $q^2 = -0.05\ (GeV/c)^2$ and for $\Delta W = 2.5\ MeV$ above threshold for $q^2 = -0.10\ (GeV/c)^2$. The results of this and all previous experiments from the 1970's [Br74, Bo77, Am70] are shown in Fig. 1. The improvement in the accuracy of the new experiment is clearly seen. The results of this experiment for A_0 compared to the predictions of chiral perturbation theory are shown in Fig. 2. The agreement is good. Since the validity of the low energy theorems is restricted to the magnitude of $|q^2| < m_\pi^2$ an extrapolation to $q^2 \to 0$ must be made for a realistic test. Based on theoretical arguments which show that the major contribution to A_0 comes from S_{0+} this multipole can be extracted from the data. The result extrapolated to $q^2 = 0$ is presented in Table 2. Within the quoted error the result is in good agreement with the predictions of the low energy theorems [Sc93] and with chiral perturbation theory [Be93] to two loops [Me94]. One notes that in the case of photoproduction, where E_{0+} is measured, that a similar approximate two loop calculation is also required to bring the theory into agreement with experiment. It appears likely that isospin breaking is needed which comes in only at the two loop level.

Although the NIKHEF experiment was a large step forward in the field the errors are rather large. This is due to the low duty factor of the accelerator (1%) which limited the total number of true π^0 events to ≈ 200. In addition the p wave contribution ($b \cdot p_\pi^{*2}$ in Eq. 5) had to be taken from a previous experiment [Br74]. The instantaneous luminosity employed at NIKHEF was $\approx 5 \cdot 10^{37} cm^{-2} s^{-1}$ (the average luminosity was $\approx 5 \cdot 10^{35} cm^{-2} s^{-1}$) which led to a raw signal to noise ratio (before cuts) of $\approx 10^{-3}$. We will improve on this by using the 100 % duty cycle accelerator MAMI and running with an average luminosity of $\approx 5 \cdot 10^{36} cm^{-2} s^{-1}$.

In spring 1994 we have performed a test experiment at $q^2 = -0.1\ (GeV/c)^2$, including a Rosenbluth separation as well as a determination of the TL interference structure function in the interval to 2 MeV above threshold. First results will be presented in Sec. 5. Recently an experiment on the threshold $p(e, e'p)\pi^\circ$ reaction at $q^2 = -0.1\ (GeV/c)^2$ was performed at NIKHEF. The coverage was up to

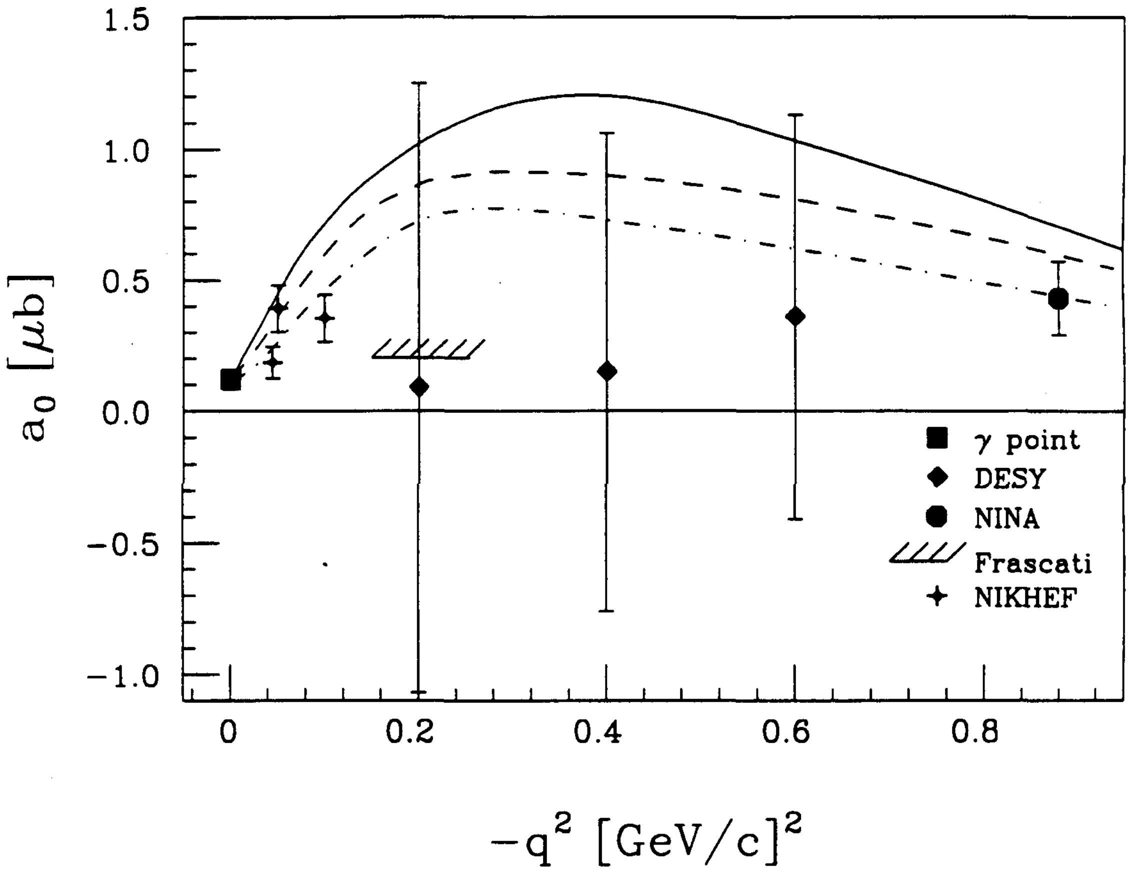

Figure 1: Plots of all data for A_0 [We 92]. The three lowest q^2 points are from NIKHEF [We 92]. The higher q^2 points with the larger errors are older data [Am70, Br74, Bo77]. The theoretical curves are from [De75, Be70, Do 72].

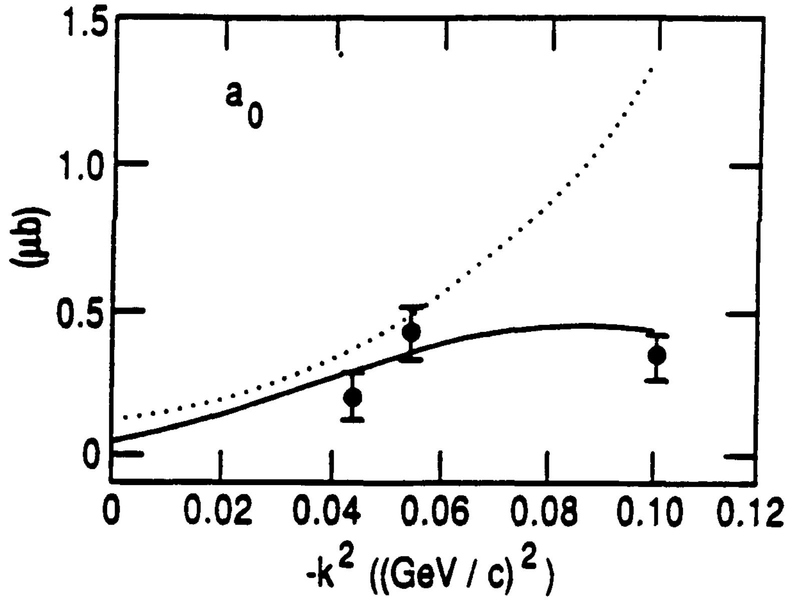

Figure 2: A_0 calculated from chiral perturbation theory [Be92] (solid curve), PV Born approximation (dotted curve) and the NIKHEF experimental data [We92].

$\approx$ $10 MeV$ above threshold and a measurement of the TL structure function was performed (no Rosenbluth separation).

The experiment proposed here will focus on $q^2 = -0.05\ (GeV/c)^2$ and emphasize the interference structure functions over a broader range of W (to 38 MeV above threshold). In particular we will obtain the first data on the $\sigma_{TL'}$ structure function by the use of polarized electrons.

4 Theoretical Predictions

In this section we will present the pertinent predictions of chiral perturbation theory [Be93, Me94] and a gauge invariant πN model [No91] which has reasonable empirical success in the Δ region [No90]. In Fig. 3 we present the predictions for $\sigma_L(\theta)$ and $\sigma_T(\theta)$ where L and T refer to the longitudinal and transverse cross sections; these predictions are for $p^*_\pi = 13\ MeV/c$ and $q^2 = -0.04\ (GeV/c)^2$. It can be seen that the predicted longitudinal cross sections are almost isotropic due to the fact that the predicted p wave longitudinal multipoles are small. On the other hand there is a dramatic difference between the prediction of chiral perturbation theory and the πN model for the transverse cross section. The reason is that in chiral perturbation theory the sign of E_{0+} is predicted to be positive while in the πN model it is predicted to be negative.

In Fig.4 we present the predicted variation of E_{0+} and S_{0+} with q^2. It can be

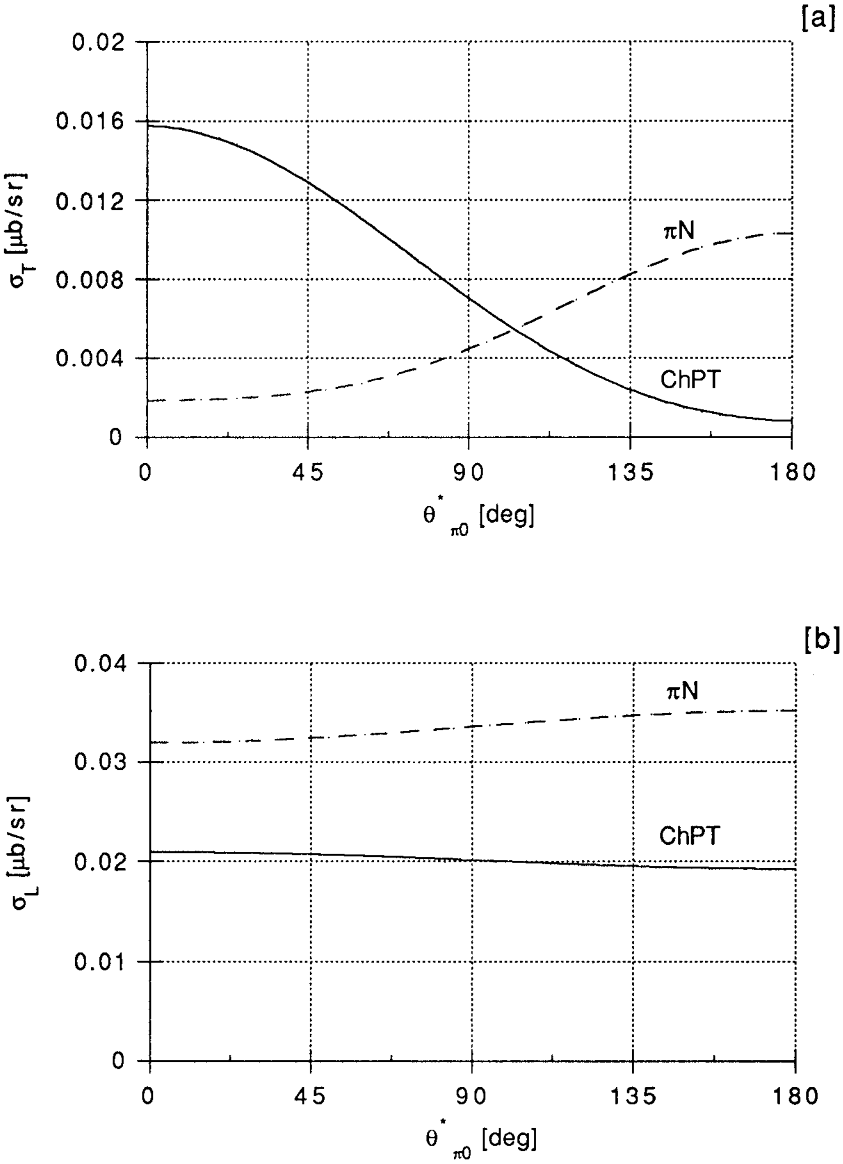

Figure 3: [a] $\sigma_T(\theta)$ and [b] $\sigma_L(\theta)$ for $W = 1074$ MeV, ($p^*_\pi = 13$ MeV/c). The solid lines are the predictions of chiral perturbation theory [Be93, Me94], the dashed lines are the predictions of a πN model [No91].

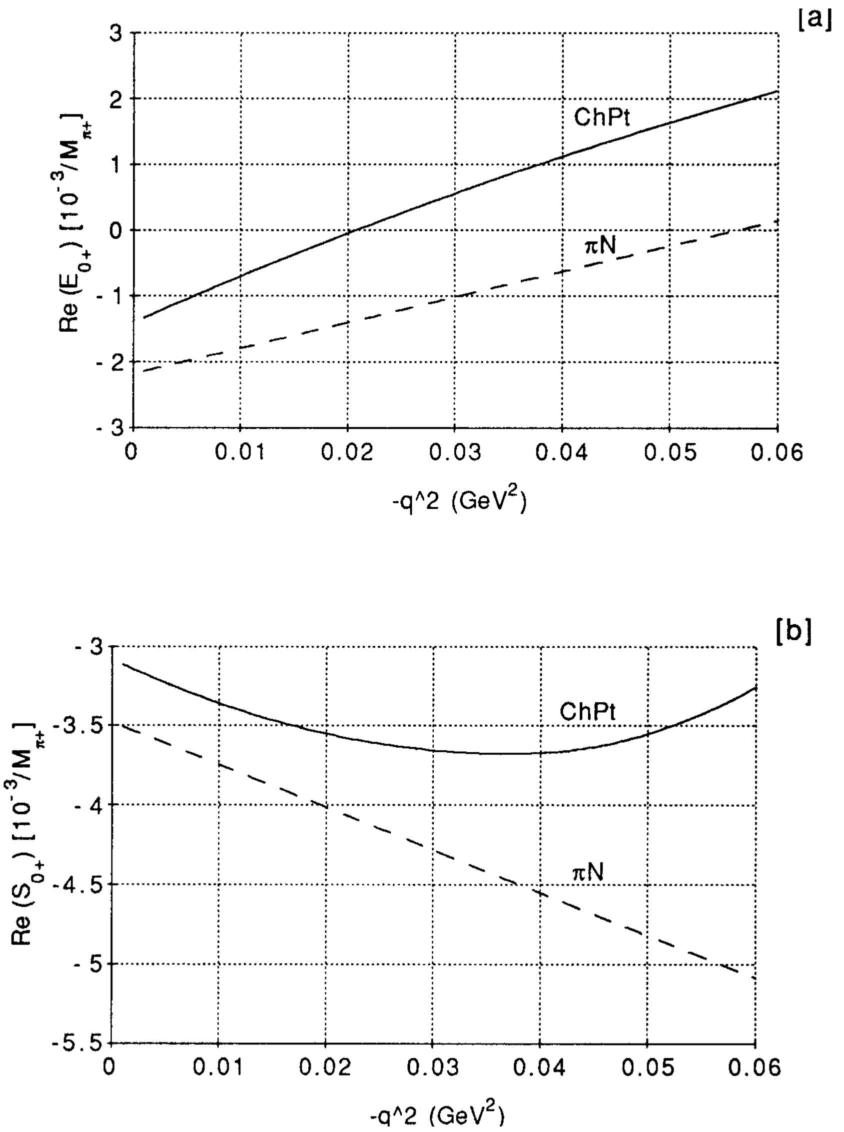

Figure 4: The real part of [a] E_{0+} and [b] S_{0+} for $W = 1074$ MeV ($p^*_\pi = 13$ MeV/c). The solid lines are the predictions of chiral perturbation theory [Be93, Me94], the dashed lines are the predictions of a πN model [No91].

seen that there is a large difference between the predictions of the πN model [No91] and chiral perturbation theory [Be93]. As part of this experiment we will measure this q^2 dependence. In Fig. 5 we present the logitudinal and transverse cross section as a function of the pion CM momentum.

In Fig. 6 we present the interference structure functions as function of θ^*_π for $p^*_\pi = 13$ MeV/c and $q^2 = -0.04$ $(GeV/c)^2$. It can be seen that the TL structure

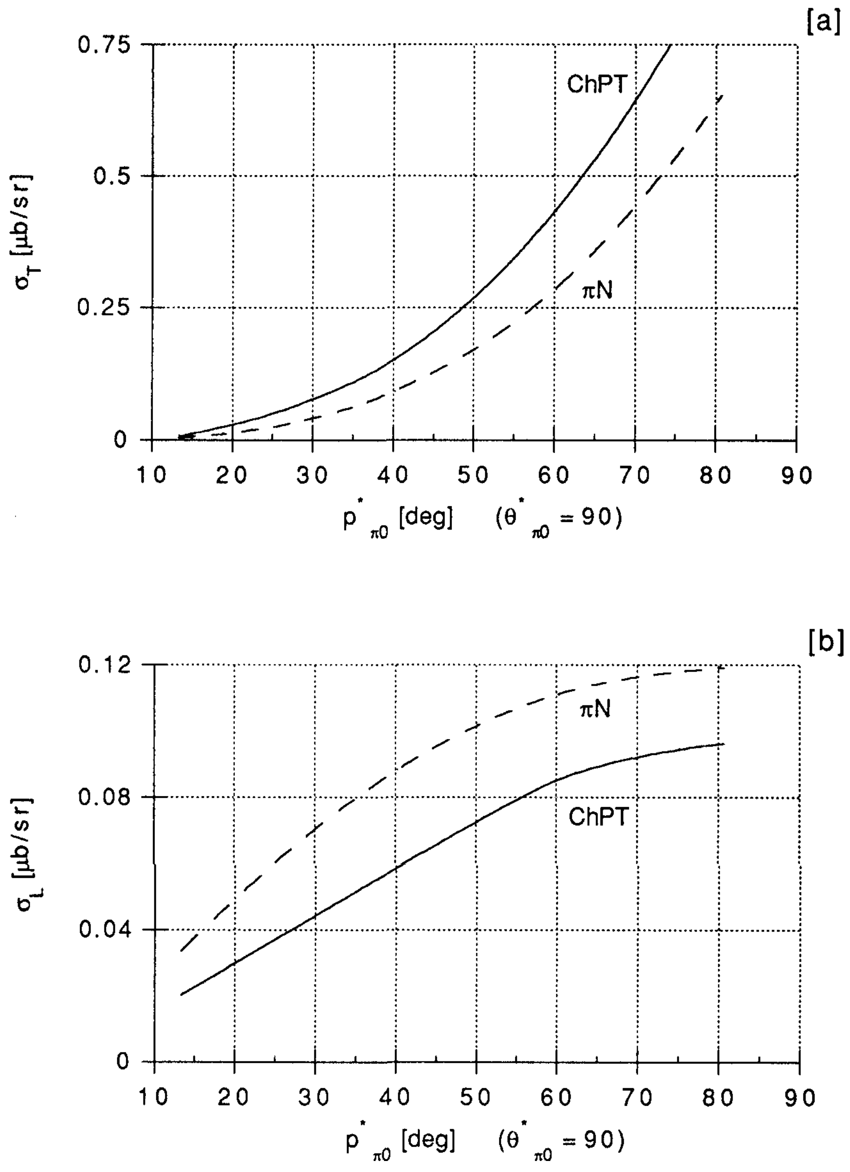

Figure 5: [a] $\sigma_T(\theta)$ and [b] $\sigma_L(\theta)$ for p^*_π for ($\theta^*_\pi = 90°$). The solid lines are the predictions of chiral perturbation theory [Be93, Me94], the dashed lines are the predictions of a πN model [No91].

function is predicted to be large, comparable to the longitudinal and transverse cross sections. The dominant contribution to the TL cross section comes from the scalar s wave multipole S_{0+} interfering with the p wave transverse multipoles E_{1+} and M_{1+}. The predictions of chiral perturbation theory for M_{1+} are very small. We suspect that this is a problem for the theory in the Δ channel. It is connected with the difficulty that chiral perturbation theory has had in predicting the magnetic nucleon polarizability [Me93]. In this connection the TT cross section is also very interesting since it is also very sensitive to the magnitude of M_{1+}.

The magnitude of the interference structure functions at 90° (close to their maximum value) are plotted versus p_π^* in Fig. 7. It can be seen that they increase rapidly. There are significant differences in the TT cross section due to differences in the predicted magnitude of M_{1+}. For the $\sigma_{TL'}$ cross section we note a significant rise above the π^+ threshold. This is due to the $\gamma_v p \to \pi^+ n \to \pi^0 p$ charge exchange reaction [Ber94]. An accurate measurement of the TL' cross section corresponds to measuring the phase shift or scattering length for the $\pi^+ n \to \pi^0 p$ charge exchange reaction. This is of interest in checking the predictions of chiral dynamics for the πN scattering lengths [We66]. It is also of great interest in checking isospin symmetry by comparing with the value of $a(\pi^- p \to \pi^0 n)$ obtained from the Panofsky ratio and the low energy theorems [Sp77]. Isospin violations due to the mass differences of the up and down quarks have been predicted for these scattering lengths [We77]. We regard this experiment as a feasibility study for the practicality of this measurement.

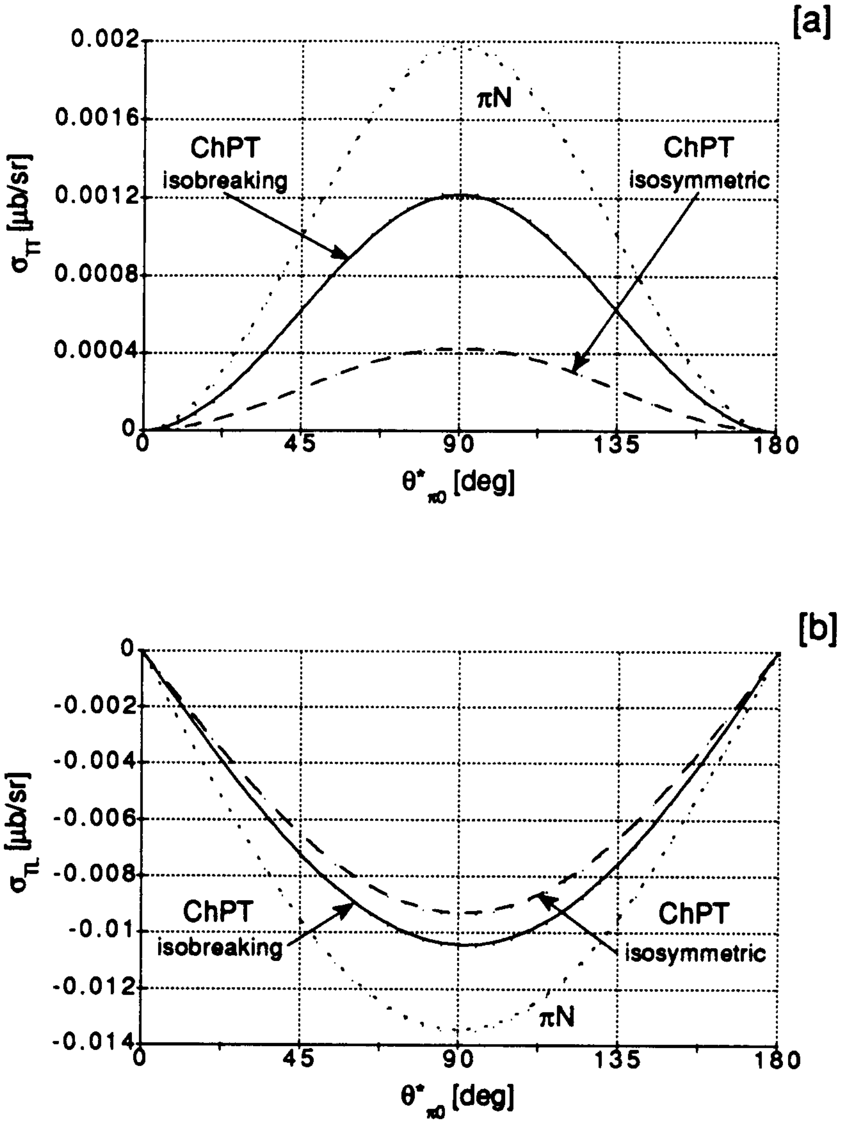

Figure 6: (a) $\sigma_{TT}(\theta)$, and (b) $\sigma_{TL}(\theta)$, versus θ^*_π for $W = 1074\ MeV$ ($p^*_\pi = 13\ MeV/c$). The solid(dashed) curves are the predictions of chiral perturbation theory with(without) isospin breaking due to the threshold difference of the electroproduction of the π^0 and π^+ channels [Be93, Me94]. The dotted curves are the predictions of a πN model [No91].

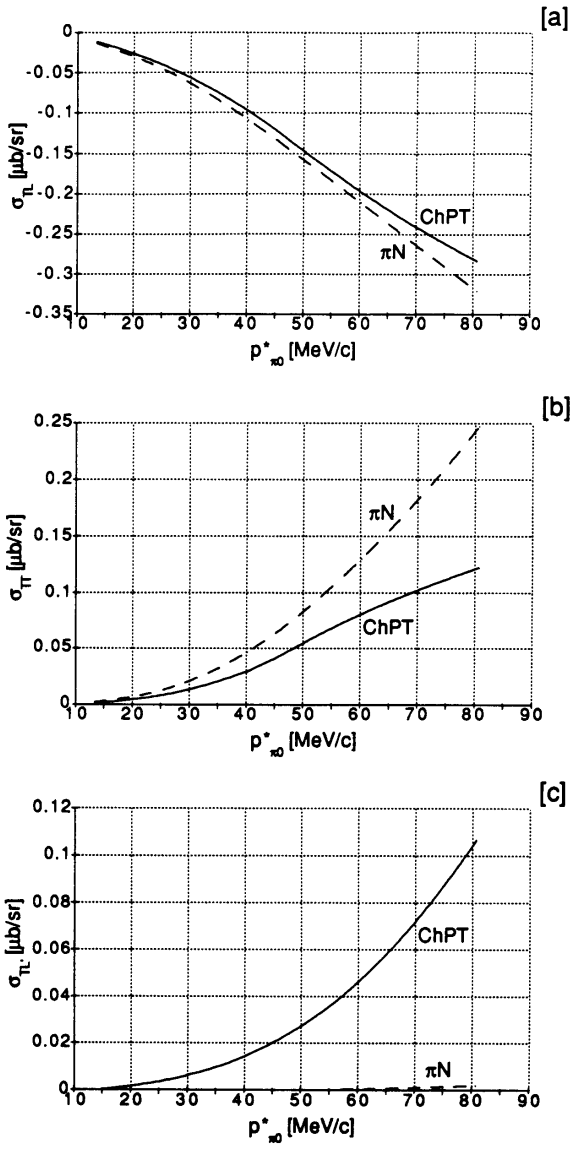

Figure 7: (a) $\sigma_{TL}(\theta^*_\pi = 90°)$, (b) $\sigma_{TT}(\theta^*_\pi = 90°)$, and (c) $\sigma_{TL'}(\theta^*_\pi = 90°)$ versus p^*_π for $W = 1074\ MeV (p^*_\pi = 13\ MeV/c)$. The solid curves are the predictions of chiral perturbation theory with isospin breaking due to the threshold difference of the electroproduction of the π^0 and π^+ channels [Be93, Me94]. The dashed curves are the predictions of a πN model [No91].

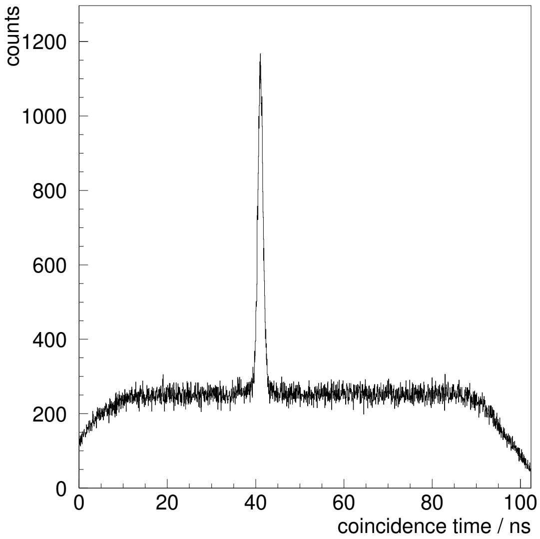

Figure 8: Coincidence time spectrum for the reaction $p(e,e'p)\pi^{\circ}$. The data was taken in february 1994. The peak has a width of 1.1 ns (FWHM).

5 Previous Test Experiment

In february 1994 we performed a first $p(e,e'p)\pi^{\circ}$ experiment to complete the test and calibration of the first two spectrometers of the Mainz 3-spectrometer-setup and to check wether the liquid hydrogen target is suitable for threshold pion production. We choosed a moderate q^2 of $-0.1(GeV/c)^2$ so that the outgoing recoil proton has a mean kinetic energy of 55 MeV. Therefore the energy loss in the long target can easily be corrected using the good vertex resolution of the electron spectrometer of about 3mm (FWHM).

The data has a very good true to random rate in the coincidence time spectrum (Fig. 8) athough the experiment has been performed with beam currents up to $22\mu A$ which correspondes to a luminosity of $1.15 \cdot 10^{37} s^{-1} cm^{-2}$. Neither target nor detector systems showed any problems to stand these high currents. After the coincidence time has been corrected for the different flight pathes in the spectrometers one ends with width of 1.1 ns (FWHM).

The π° was not detected directly but the scattered electron and the recoil proton. So all kinematical variables of the reaction are measured and the π° can be identified by the 'missing mass'. Fig. 9 shows such a spectrum with a peak exactly at 135 MeV and a width of 2 MeV.

To measure the $\sigma_{TL}$and σ_{TT}cross section one needs a good angular resolution in the CM system of the proton and the pion. Fig. 10 shows the lab momentum of the proton versus the lab angle of the proton relativ to the direction of the momentum

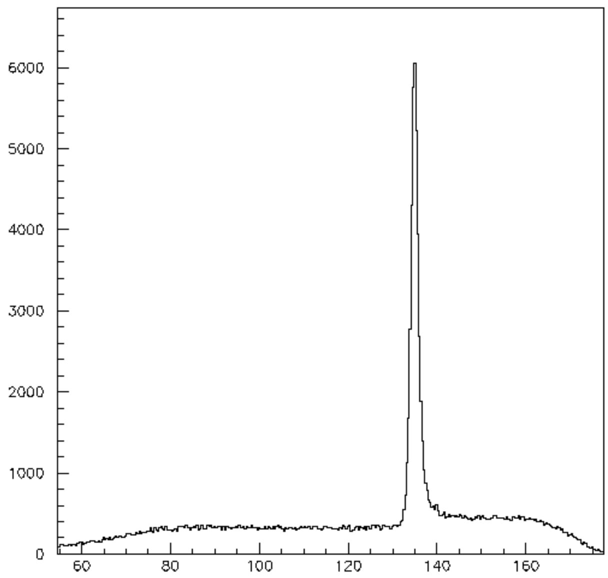

Figure 9: 'missing mass' spectrum of the reaction $p(e, e'p)\pi^{\circ}$. The center of the peak is at 135 MeV with a width of 2 MeV. This is how the π° is identified.

transfer. Data with an invariant mass of $1MeV < \Delta W < 2MeV$ above threshold is accumulated. This plot can be compared to the proton kinematics shown in Fig. 12. The achieved angular resolution in CM system of pion and the nucleon is about $\Delta\Theta^*_{\pi} \simeq 10^{\circ}$.

Because things went so well the data will be analysed further. In particular a seperation of the $\sigma_L$and $\sigma_T$cross section will be performed [Di94].

6 Spectrometers and Calibration

Many technical details and the performance of Mainz 3-spectrometer-setup are described in the annual reports [Ja90] and [Ja92]. Therefore we limit our to some details that effect this particular beam time request.

All three spectrometers are equiped with a very similar detector system, which consists of four plane of vertical driftchamber, two planes of scintillators and a gas Cerenkov detector. The detectors, most of the electronics as well as the data aquisition can be checked using cosmic rays during the setup without beam. Even the Cerenkov detector and the coincidence electronics can be setup without beam using a laser monitoring system which provides light pulses to all trigger detectors. Therefore only a few hours of beam time are needed to do some fine tuning.

The main part of the setup time is needed to install the liquid hydrogen target. The support for the cooling machine can be build up in about one working week.

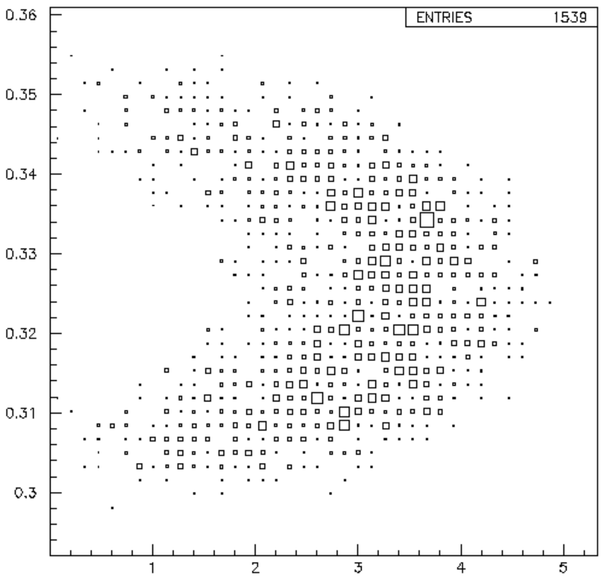

Figure 10: This plot shows the proton momentum (GeV) versus the laboratory angle of the proton relativ to the direction of the momentum transfer (degrees). Data with an invariant mass of $1MeV < \Delta W < 2MeV$ above threshold is accumulated. One can conclude from this plot, that the angular resolution in CM system of pion and the nucleon is about $\Delta\Theta^*_\pi \simeq 10°$.

Of course the setup time without beam can be cut down if a previous experiment uses the liquid hydrogen target as well.

Prior to every setup we plan to do some calibration measurements. For every spectrometer we will verify the experimental raytracing using a sieve slit as a collimator and do an elastic scattering experiment off a ^{181}Ta target. The alignment and the energy calibration of the spectrometers can be checked doing an elastic scattering measurement off the hydrogen. This calibration will take about 5 hours for each setup.

The run schedule has been optimized to avoid energy changes of the MAMI accelator and field changes of the spectrometers. 4 hours (20 minutes) have been taken into account respectively.

7 Experiment and Count Rate Estimates

For the count rate estimates we used the multipoles of [Me94] given for

$$q^2 = -0.04\ (GeV/c)^2$$

This model should slightly underestimate the cross section at $q^2 = -0.05\ (GeV/c)^2$. The kinematics and cross section formulas were calculated at $q^2 = -0.05\ (GeV/c)^2$. Fig. 11 shows the predicted structure functions of this model.

The laboratory kinematics of the outgoing protons are shown in Fig. 12. For each pion CM energy there are two laboratory proton energies at each laboratory angle. These must be distinguished to know which proton is emitted forwards or backwards in the CM system. For higher CM momenta the opening cone angle of the emitted protons exceeds the spectrometer acceptance. In addition as p^*_π increases the q vector moves towards the beam line. Therefore one must move the proton spectrometer to measure an extended kinematical region. The previously performed experiments did not make these adjustments and were therefore limited in their kinematical coverage. In order to handle this kinematical problem we plan to employ the proton and electron spectrometer in several different angular and momentum settings.

Tables 3, 4 and 5 show the chosen settings and the expected total count rates. The quoted count rates were calculated with

$$\begin{aligned} \text{Luminosity: } L &= 5 \cdot 10^{36}\ \frac{Hz}{cm^2} \\ \text{Target length: } l &= 1\ cm \\ \text{Current: } I &= 19\ \mu A \\ \text{Binning: } \Delta q^2 &= 0.01\ (GeV/c)^2 \\ \text{Pion Momentum: } p^*_\pi &< 100\ MeV/c \end{aligned}$$

The resulting run schedule including calibration and setup time is given in Appendix B.

Near threshold we expect a smooth angular distribution of σ_L and σ_T in the form

$$A + B\cos\theta + C\cos^2\theta$$

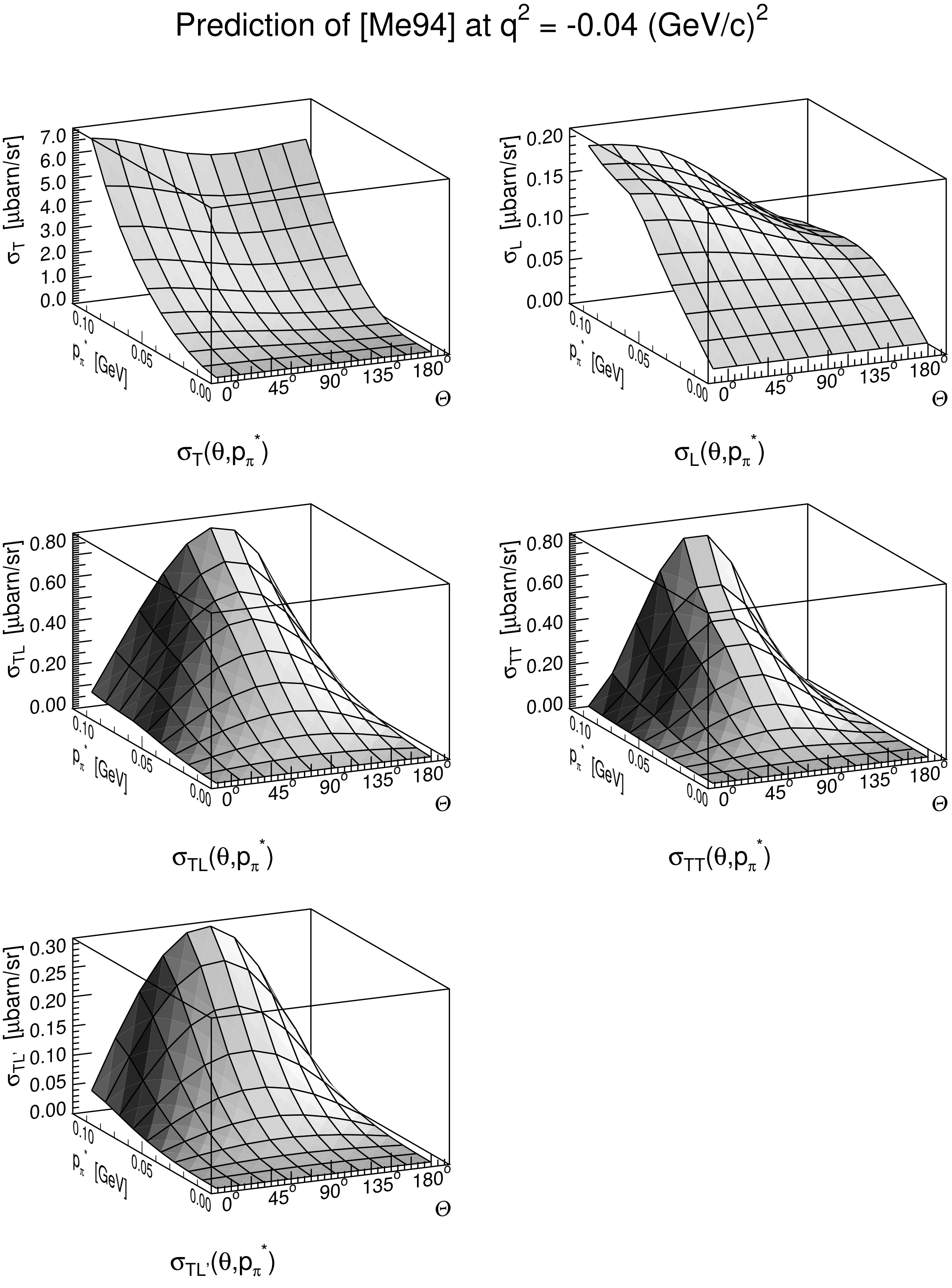

Figure 11: The prediction of chiral perturbation theory [Me94] for $q^2 = -0.04(GeV/c)^2$, used for the count rate estimates.

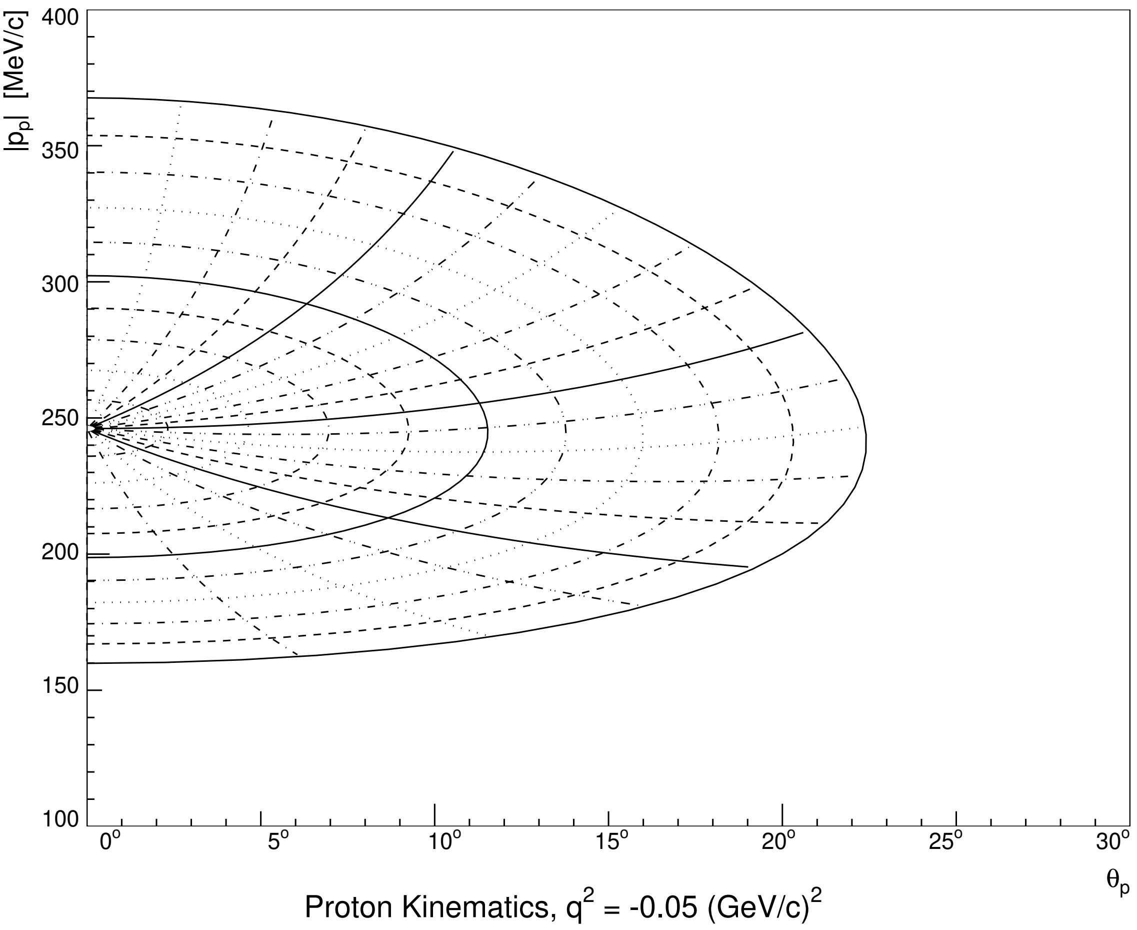

Figure 12: Proton momenta versus laboratory angle for the $p(\vec{e}, e'p)\pi^0$ reaction at $q^2 = -0.05\ (GeV/c)^2$ as a function of the pion CM momenta $p^*_\pi < 100 MeV/c$ (in steps of 10 MeV/c) and θ^*_π (in steps of 10°).

In Plane Measurement and Rosenbluth Separation								
	θ_B	θ_A	Momentum MeV/c	E_{Beam} MeV	p^*_π MeV/c	θ^*_π	ϕ^*_π	Counts $\times 10^3$
$\epsilon \approx 0.94$								
0-1	17.193°	40.1°	155 - 189	855	80	180°		26.8 in 10h
0-2	16.913°	43.4°	186 - 228	855	40	180°		49.4 in 10h
0-3	16.818°	44.6°	225 - 275	855	0			66.5 in 20h
0-4	16.913°	43.4°	261 - 319	855	40	0°		60.3 in 10h
0-5	17.193°	40.1°	303 - 370	855	80	0°		68.7 in 5h
0-6	17.193°	22.1°	241 - 295	855	80	90°	180°	59.3 in 5h
0-7	16.913°	34.4°	226 - 275	855	40	90°	180°	66.7 in 10h
0-8	16.913°	52.4°	226 - 275	855	40	90°	0°	53.4 in 10h
0-9	17.193°	58.1°	241 - 295	855	80	90°	0°	58.5 in 10h
$\epsilon \approx 0.50$								
1-1	65.522°	23.1°	155 - 189	330	80	180°		2.4 in 20h
1-2	60.105°	27.2°	186 - 228	330	40	180°		10.0 in 10h
1-3	58.496°	28.7°	225 - 275	330	0			11.4 in 20h
1-4	60.105°	27.2°	261 - 319	330	40	0°		12.5 in 10h
1-5	65.522°	23.1°	303 - 370	330	80	0°		32.5 in 10h
1-6	60.105°	36.2°	226 - 275	330	40	90°	0°	9.2 in 10h
1-7	65.522°	41.1°	241 - 295	330	80	90°	0°	16.7 in 10h

Table 3: Settings to measure the in plane structure functions at $q^2 = -0.05$ with Rosenbluth separation. Setting 0-1 through 0-9 uses spectrometer B, 1-1 through 1-7 spectrometer C for the electron arm.

q^2 Dependency of Total Cross Section							
	θ_B	θ_A	Momentum MeV/c	E_{Beam} MeV	ϵ	q^2 GeV^2/c^2	Counts $\times 10^3$
2-1	15.285°	35.2°	165 - 201	615	0.93	-0.02	22.6 in 10h
2-2	14.973°	43.2°	204 - 250	855	0.94	-0.04	39.5 in 10h
2-3	18.509°	45.5°	238 - 290	855	0.93	-0.06	28.4 in 10h
2-4	21.576°	46.4°	267 - 326	855	0.91	-0.08	22.3 in 10h
2-5	24.357°	46.6°	293 - 359	855	0.89	-0.10	19.8 in 10h
3-1	34.259°	27.9°	165 - 201	330	0.70	-0.02	12.9 in 10h
3-2	50.916°	29.3°	202 - 250	330	0.57	-0.04	14.9 in 20h
3-3	65.974°	27.6°	238 - 290	330	0.44	-0.06	10.8 in 20h
3-4	81.344°	24.6°	267 - 326	330	0.32	-0.08	9.0 in 20h
3-5	98.488°	20.5°	293 - 359	330	0.21	-0.10	10.2 in 30h

Table 4: Settings to measure the q^2 dependence of the threshold cross section in the range $0.01 < q^2 < 0.1$ with Rosenbluth separation. Setting 2-1 through 2-5 uses spectrometer B, 3-1 through 3-5 spectrometer C for the electron arm.

Out of Plane Measurement with Polarized Beam									
	θ_B	θ_A	Momentum MeV/c	E_{Beam} MeV	p^*_π MeV/c	α_{OOP}	θ^*_π	ϕ^*_π	Counts $\times 10^3$
4-1	15.443°	40.1°	239 - 298	855	80	7.65°	90°	90°	30.8 in 10h
4-2	16.456°	43.4°	225 - 280	855	40	3.96°	90°	90°	41.0 in 10h
4-3	16.818°	44.6°	222 - 271	855	0	0°	90°		33.6 in 10h
4-4	16.913°	52.4°	226 - 275	855	40	0°	90°	0°	53.4 in 10h
4-5	17.193°	58.1°	241 - 295	855	80	0°	90°	0°	58.5 in 10h

Table 5: Settings to measure the out of plane dependend structure functions with polarized electron beam.

(See Appendix A). To accuratly determine the coefficients (A,B,C) of this distribution it is sufficient to measure the in plane cross section at $\theta_\pi^* = 0°$, $90°$, and $180°$. This will be done in settings 0-1 through 0-7.

σ_{TL} has the distribution

$$sin\theta \cos\phi$$

(we expect the p-wave - p-wave interference to be negligible compared to the s-wave-p-wave interference). So we measure this structure function by measuring the cross section at $\theta_\pi^* = 90°, \phi = 0°, 180°$ (Settings 0-6 through 0-9).

To separate σ_L and σ_T we measure the same cross section at $\epsilon \approx 0.50$ (Rosenbluth separation). At this point we already now σ_{TL} so it is not necessary to repeat setting 0-6 and 0-7 for this measurement, which is impossible due to the small needed angle of spectrometer A. For the electron arm we use in setting 1-1 through 1-7 spectrometer C with a larger acceptance in the scattering plane.

For the measurement of σ_{TT} and $\sigma_{TL'}$ we use the out of plane capability of spectrometer B. An out of plane shift of B of 7.65° corresponds to an out of plane angle of 18° for the virtual photon direction. The maximum laboratory angle of the proton is $\theta_p = 21°$ for $\theta_\pi^* = 90°$ so this measurement can cover the full range at $\phi_\pi^* = 90°$, $\theta_\pi^* = 90°$ (settings 4-1,4-2). In setting (4-3 - 4-5) we repeat the in plane measurement at $\phi_\pi^* = 0°$, $\theta_\pi^* = 90°$ to reduce systematic errors by measuring the asymmetry in one run under same conditions. This measurement is also necessary to separate σ_T and σ_{TT} which cannot be separated by an in plane measurement.

In setting 2-1 through 2-5 and 3-1 through 3-5 we measure the q^2 dependence of the E_{0+} and L_{0+} multipole. We want to determine the change of sign of E_{0+} which is known to be positive at $-q^2 > 0.1$ and negative at the photon point. We include the point $q^2 = -0.02\ (GeV/c)^2$ although we expect a larger error by multiple scattering and energy loss of the low energy proton for this point.

To illustrate the kinematical coverage by different angle settings we present in Fig. 13 the count rates for one momentum (30 MeV/c) for five different settings. The sum of this five settings will give nearly full coverage of the angular range with total counts of ≈ 600 per bin by a 10×10 binning in the pion direction. In the further analysis this ≈ 60000 events will be reduced to the six coefficients of the smooth angular distribution

$$A \ + \ B \cdot \cos\theta \ + \ C \cdot \cos^2\theta \ + \ D \cdot \sin^2\theta \cos 2\phi \ + \ E \cdot \sin\theta \cos\phi \ + \ F \cdot \sin\theta \sin\phi$$

so the statistical error will be less than 1% of the leading term. We expect, that the statistical error will be smaller than the systematic error by background subtraction. At higher pion momenta the count rates are higher due to the increase of the cross section, at lower pion momenta the kinematical coverage is larger due to the kinematical focussing on the spectrometer acceptance.

Appendic C shows the energy loss calculations for the lowest momentum (155 MeV/c). The protons can leave the target and reach the detectors, the momentum resolution is sufficient. For typical momenta (246 MeV/c at threshold) the momentum resolution by energy loss is better than 3 MeV, the multiple scattering causes an error less than 3°.

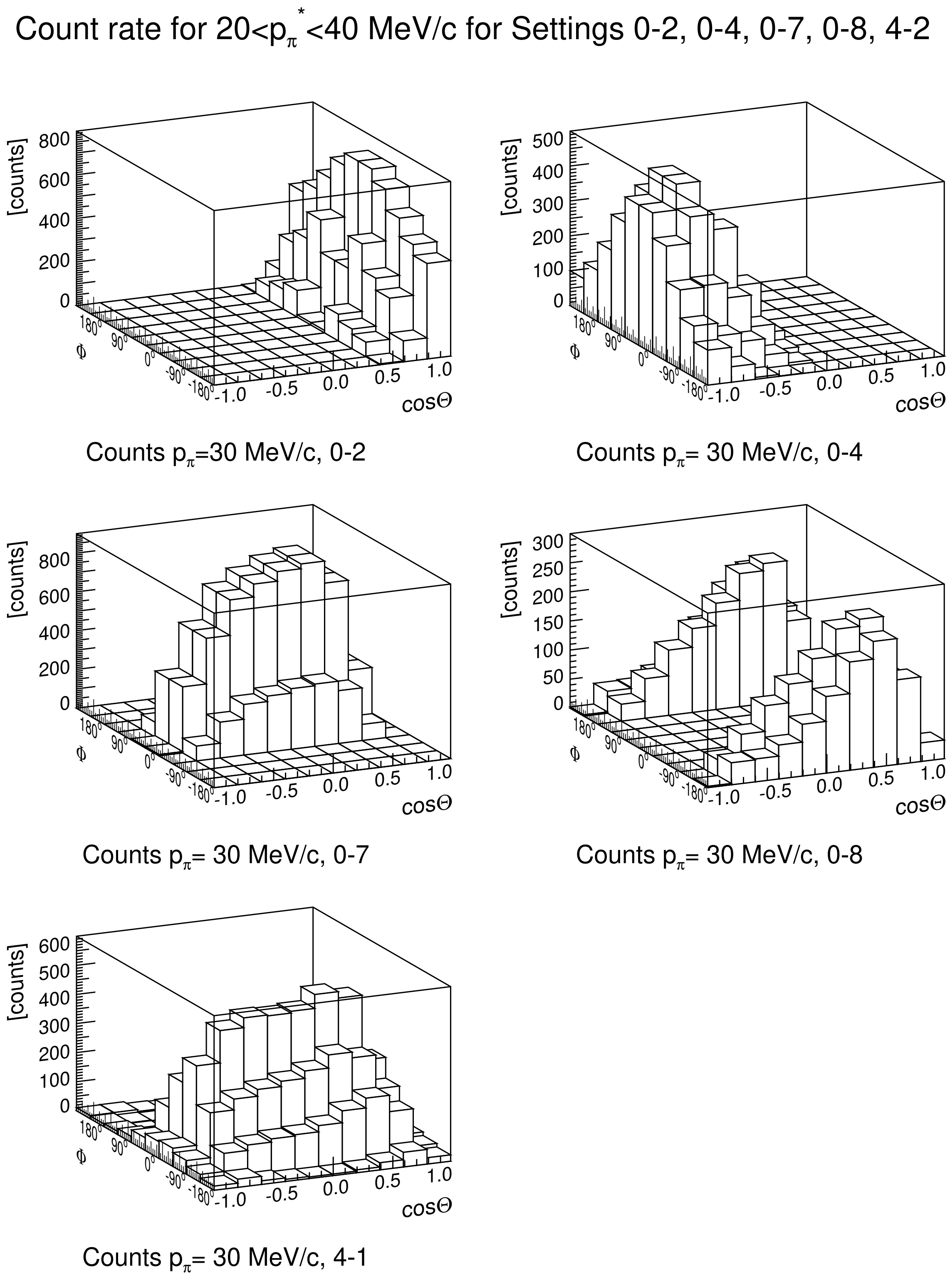

Figure 13: Counts in the momentum range $p_\pi^* = 30 \pm 10\ MeV/c$ for different momentum and angular settings.

Conclusion

With our unique experimental equipment it is possible to measure accurately all of the structure functions σ_L, σ_T, σ_{TT}, σ_{TL} and $\sigma_{TL'}$ of the reaction $p(\vec{e}, e'p)\pi^0$ with large kinematical coverage. We have designed this experiment as a stringent test of the predictions of chiral dynamics. This is of particular significance since this theory is suggested to be an accurate approximation to QCD at the confinement scale.

References

[Ad68] S. L. Adler and R. Dashen, Current Algebras and Applications to Particle Physics, Benjamin, NY (1968).

[Am70] E. Amaldi *et al.*, Nuovo Cimento **65A**, 377 (1970).

[Am79] E. Amaldi, S. Fubini, and G. Furlan, Pion-Electroproduction, Springer Tracts in Modern Physics #83 (1979).

[Be70] G. Benfatto, F. Nicolo and G. C. Rossi, Nucl. Phys. **B50**, 205 (1970) and Nuovo Cimento, **14A**, 425 (1973).

[Be92] V. Bernard, N. Kaiser, Ulf-G. Meißner, Nucl. Phys. **B383**, 442 (1992).

[Be93] V. Bernard, N. Kaiser, T.-S. H. Lee, Ulf-G. Meißner, Phys. Rev. Lett. **70**, 387 (1993).

[Bec90] R. Beck *et al.*, Phys. Rev. Lett. **65**, 1841 (1990).

[Ber91] A. M. Bernstein, B. R. Holstein, Comm. Nucl. Part. Phys. **20**, 197 (1991).

[Ber94] A.M.Bernstein, to be published.

[Bo77] D. R. Botterill *et al.*, Nucl. Phys **B116**, 65 (1977).

[Br74] P. Brauel *et al.*, Phys. Lett. **50B**, 507 (1974).

[De75] R. C. E. Devenish and D. H. Lyth, Nucl. Phys. **B93**, 108 (1975).

[deB70] P. de Baenst, Nucl. Phys. **B24**, 633 (1970).

[Di94] M. O. Distler, Doctorate thesis, Mainz 1994

[Do 72] N. Donbey and B. J. Read, Nucl. Phys. **B60**, 65 (1972).

[Do92] Dynamics of the Standard Model, J.F.Donoghue, E.Golowich, and B.R.Holstein, Cambridge University Press (1992).

[Ja90] Jahresbericht 1990/91, Institut für Kernphysik, Universität Mainz

[Ja92] Jahresbericht 1992/93, Institut für Kernphysik, Universität Mainz

[Ma86] E. Mazzucato *et al.*, Phys. Rev. Lett. **57**, 3144 (1986).

[Me93] Ulf-G. Meißner, Rep. Prog. Phys. **56**, 903 (1993).

[Me94] Ulf-G. Meißner, private communication

[Na91] H. W. L. Nauss, Phys. Rev. **C43**, R365 (1991)
H. W. L. Nauss, J. H. Koch, and J. L. Friar, Phys. Rev. **C41**, 2852 (1990).

[No90] S. Nozawa and T. S. H. Lee, Nucl. Phys. **A513**, 511 (1990), and **A513**, 543 (1990).

[No91] S. Nozawa, private communication.

[Ra89] A. S. Raskin and T. W. Donnely, Ann. of Phys. **191**, 78 (1989).

[Sc93] S.Scherer, J.H.Koch, and J.L.Friar, Nucl. Phys. **A552**, 515 (1993).

[Sp77] J. Spuller *et al.*, Phys. Lett. **67B**, 478 (1977).

[We 92] T. P. Welch *et. al.*, Phys. Rev. Let. **69**, 2761 (1992).

[We66] S. Weinberg, Phys. Rev. Lett. **17**, 168 (1966)

[We77] S. Weinberg, Transactions of the New York Academy of Science, Series II **38** (I. I. Rabi Festschrift), 185 (1977).

[We79] S. Weinberg, Physica (Amsterdam) **96A**, 327 (1979).
J. Gasser and H. Leutwyler, Ann. Phys. (N.Y.) **158**, 142 (1984).

[We92] T. P. Welch, Ph. D. Thesis, University of Virginia (1992).

Appendix A

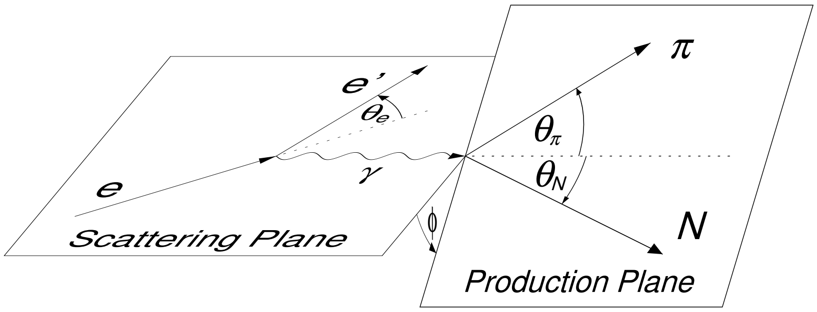

Cross section decomposition [Ra89]:

$$\begin{aligned}\frac{d^3\sigma}{d\Omega_e dE' d\Omega_\pi^*} &= \Gamma_t(\sigma_T(\theta) + \epsilon\sigma_L(\theta) + \epsilon\sigma_{TT}(\theta)\cos 2\phi \\ &+\sqrt{2\epsilon(1+\epsilon)}\sigma_{TL}(\theta)\cos\phi + h\sqrt{2\epsilon(1-\epsilon)}\sigma_{TL'}(\theta)\sin\phi)\end{aligned}$$

$$\begin{aligned}\epsilon &= \left(1 - \tfrac{2(\omega^2-q^2)}{q^2} tan^2\tfrac{\theta_e}{2}\right)^{-1} & \Gamma_t &= \tfrac{\alpha}{2\pi^2}\tfrac{E'}{E}\tfrac{k_\gamma}{(-q^2)}\tfrac{1}{1-\epsilon} \\ k_\gamma &= \tfrac{W^2-M_p^2}{2M_p} & k_\gamma^* &= \tfrac{M_p}{W}k_\gamma = \tfrac{W^2-M_p^2}{2W}\end{aligned}$$

Multipole decomposition of the structure functions up to $l = 1$:

$$\begin{aligned}\sigma_T &= \frac{p_\pi^*}{k_\gamma^*}(|E_{0+}|^2 + \frac{1}{2}|2M_{1+} + M_{1-}|^2 + \frac{1}{2}|3E_{1+} - M_{1+} + M_{1-}|^2 \\ &+2\cos\theta\ Re\{E_{0+}^*(3E_{1+} + M_{1+} - M_{1-})\} + \cos^2\theta\ (|3E_{1+} + M_{1+} - M_{1-}|^2 \\ &-\frac{1}{2}|2M_{1+} + M_{1-}|^2 - \frac{1}{2}|3E_{1+} - M_{1+} + M_{1-}|^2)) \\ \sigma_L &= \frac{-q^2}{\omega^{*2}}\frac{p_\pi^*}{k_\gamma^*}(|L_{0+}|^2 + 4|L_{1+}|^2 + |L_{1-}|^2 - 4Re\{L_{1+}^*L_{1-}\} \\ &+2\cos\theta\ Re\{L_{0+}^*(4L_{1+} + L_{1-})\} + 12\cos^2\theta(|L_{1+}|^2 + Re\{L_{1+}^*L_{1-}\})) \\ \sigma_{TL} &= \sqrt{\frac{-q^2}{\omega^{*2}}}\frac{p_\pi^*}{k_\gamma^*}(-\sin\theta\ Re\{L_{0+}^*(3E_{1+} - M_{1+} + M_{1-}) - (2L_{1+}^* - L_{1-}^*)E_{0+} \\ &+6\cos\theta(L_{1+}^*(E_{1+} - M_{1+} + M_{1-}) + L_{1-}^*E_{1+})\}) \\ \sigma_{TT} &= \frac{p_\pi^*}{k_\gamma^*}(3\sin^2\theta(\frac{3}{2}|E_{1+}|^2 - \frac{1}{2}|M_{1+}|^2 - Re\{E_{1+}^*(M_{1+} - M_{1-}) + M_{1+}^*M_{1-}\}) \\ \sigma_{TL'} &= \sqrt{\frac{-q^2}{\omega^{*2}}}\frac{p_\pi^*}{k_\gamma^*}(\sin\theta\ Im\{L_{0+}^*(3E_{1+} - M_{1+} + M_{1-}) - (2L_{1+}^* - L_{1-}^*)E_{0+} \\ &+6\cos\theta(L_{1+}^*(E_{1+} - M_{1+} + M_{1-}) + L_{1-}^*E_{1+})\})\end{aligned}$$

Appendix B: Run schedule

Run 1 (8.3 days)					
	θ_e	θ_A	p_A MeV/c	E_{Beam} MeV	Time
Calibration Spectrometer A and B					5h
0-5	17.193°	40.1°	337	855	5h + 20'
0-4	16.913°	43.4°	290	855	10h + 20'
0-6	17.193°	22.1°	268	855	5h + 20'
0-9	17.193°	58.1°	268	855	10h + 20'
0-3	16.818°	44.6°	250	855	20h + 20'
0-7	16.913°	34.4°	250	855	10h + 20'
0-8	16.913°	52.4°	250	855	10h + 20'
0-2	16.913°	43.4°	207	855	10h + 20'
0-1	17.193°	40.1°	172	855	10h
Sum					98h
Energy Change					4h
Calibration Spectrometer A and C					5h
1-5	65.522°	23.1°	337	330	10h + 20'
1-4	60.105°	27.2°	290	330	10h + 20'
1-7	65.522°	41.1°	268	330	10h + 20'
1-3	58.496°	28.7°	250	330	20h + 20'
1-6	60.105°	36.2°	250	330	10h + 20'
1-2	60.105°	27.2°	207	330	10h + 20'
1-1	65.522°	23.1°	172	330	20h
Sum					97h
Total					199h (=8.3d)

Run 2 (6.3 days)					
	θ_B	θ_A	p_A MeV/c	E_{Beam} MeV	Time
2-5	24.357°	46.6°	326	855	10h+20'
2-4	21.576°	46.4°	297	855	10h+20'
2-3	18.509°	45.5°	264	855	10h+20'
2-2	14.973°	43.2°	227	855	10h
Energy Change					4h
3-5	98.488°	20.5°	326	330	30h+20'
3-4	81.344°	24.6°	297	330	20h+20'
3-3	65.974°	27.6°	264	330	20h+20'
3-2	50.916°	29.3°	227	330	20h+20'
3-1	34.259°	27.9°	184	330	10h
Energy Change					4h
2-1	15.285°	35.2°	184	615	10h
Total					150h (=6.3d)

Run 3 (2.2 days), polarized Beam					
	θ_B	θ_A	p_A MeV/c	E_{Beam} MeV	Time
4-1	15.443°	40.1°	267	855	10h+1h'
4-2	16.456°	43.4°	253	855	10h+1h'
4-5	17.193°	58.1°	268	855	10h+20'
4-4	16.913°	52.4°	251	855	10h+20'
4-3	16.818°	44.6°	247	855	10h
Total					53h (=2.2d)

Appendix C: Energy Loss

The following table presents an energy loss calculation for the lowest proton momentum, including all foils and materials.

	x [mm]	$\frac{dE}{dx} \cdot x$ [MeV]	p [MeV/c]	E_{kin} [MeV]	β	$\Delta\theta$
Initial value			155	12.80	0.163	
Target	5	-2.89	134	9.52	0.141	0.21°
Havar (Target cell)	0.007	-0.17	132	9.35	0.140	0.21°
Kapton (Vacuum chamber)	0.120	-0.77	127	8.55	0.134	0.21°
Air	50	-0.29	124	8.25	0.131	1.20°
Kapton (Spectrometer in)	0.120	-0.85	117	7.35	0.124	1.20°
Kapton (Spectrometer out)	0.077	-0.60	112	6.72	0.119	1.20°
Air	200	-1.42	098	5.15	0.104	16.30°
Mylar (Wirechambers)	0.018	-0.18	096	4.96	0.102	16.30°

The protons can reach the detectors and can be detected. The momentum resolution is determined by the uncertainty of the vertex inside the target. The maximum uncertainty is about 10 MeV/c. At the low momentum point we cover only a small kinematical region, so the angular resolution of $\Delta\theta = 16.30°$ is not critical.